Journal of Power Sources 342 (2017) 1017–1031

Contents lists available at ScienceDirect

Journal of Power Sources

journal homepage: www.elsevier.com/locate/jpowsour

Modeling of microfluidic microbial fuel cells using quantitative bacterial transport parameters

Mohammad Mahdi Mardanpour [a, b], Soheila Yaghmaei [b, *], Mohammad Kalantar [b]

[a] Technology and Innovation Group, Research Institute of Petroleum Industry, Tehran, Iran
[b] Department of Chemical and Petroleum Engineering, Sharif University of Technology, Tehran, Iran

HIGHLIGHTS

- The dynamic modeling of microfluidic microbial fuel cell was presented.
- The model predictions with the experimental data coincide appropriately.
- As the diameter of microchannel is decreased, the produced power increases.
- The system performance was assessed by analyzing the biofilm and anolyte features.

ARTICLE INFO

Article history:
Received 20 October 2016
Received in revised form
12 December 2016
Accepted 3 January 2017
Available online 13 January 2017

Keywords:
Microfluidic microbial fuel cell
Modeling
Bacterial transport parameters
Chemotaxis

ABSTRACT

The objective of present study is to analyze the dynamic modeling of bioelectrochemical processes and improvement of the performance of previous models using quantitative data of bacterial transport parameters. The main deficiency of previous MFC models concerning spatial distribution of biocatalysts is an assumption of initial distribution of attached/suspended bacteria on electrode or in anolyte bulk which is the foundation for biofilm formation. In order to modify this imperfection, the quantification of chemotactic motility to understand the mechanisms of the suspended microorganisms' distribution in anolyte and/or their attachment to anode surface to extend the biofilm is implemented numerically. The spatial and temporal distributions of the bacteria, as well as the dynamic behavior of the anolyte and biofilm are simulated. The performance of the microfluidic MFC as a chemotaxis assay is assessed by analyzing the bacteria activity, substrate variation, bioelectricity production rate and the influences of external resistance on the biofilm and anolyte's features.

1. Introduction

Chemotaxis refers to bacteria's ability to detect and respond to extracellular changes in their environment by biased random motion. When bacteria experience favorable chemical gradients, tumbles are suppressed [1,2], resulting in a net chemotactic drift toward an attractant or away from a repellent as a three-dimensional random walk [3].

The chemotaxis of free-swimming or surface-adhering bacterial cells plays a fundamental role in microbial population dynamics, biofilm formation and dispersion [4]. Therefore, the quantitative data of microbial transport parameters is essential to predict the strength of attraction of a bacterial population to given chemical gradients.

The intrinsic advantages of microfluidic microbial fuel cells (MFCs) result from the scale-dependent processes of transport phenomena that provide a powerful platform for the investigation of biological phenomena with unique features such as cost and time-efficient opportunities, high precision and exquisite control over the experimental parameters, leading to high reproducibility amongst separate devices are undeniable [5]. Any variations in the concentration and/or organic content of the MFC fed, is directly proportional to the amount of generated electrons and therefore the output current. In addition, the variations of microbial population can be observed during current evolutions of microfluidic MFC. Thus, MFC-type as amperometric biosensors prove to be a valid alternative to traditional biosensors for screening biological and biochemical processes in simple to complex substrates [6].

* Corresponding author.
E-mail address: yaghmaei@sharif.edu (S. Yaghmaei).

http://dx.doi.org/10.1016/j.jpowsour.2017.01.012
0378-7753/

2. Literature review

In the context of microfluidic MFC modeling, the foundation of a conventional MFC model relies on the electron transfer mechanisms (including mediator based [7], and conduction based [8,9]), and microorganisms' populations, including pure [9] and mixed [10] cultures. The simulation of microbial populations plays a significant role in ensuring the accuracy and extension of the predicted results. The main assumption in majority of the earlier MFC models was that the development of next generation of microorganisms administered was considered to be based on the initial biofilm distribution. The suitableness of this initial distribution was assessed on the basis of coinciding with the final experimental data of sustained situations (i.e. the current evolutions [7] and polarization curves [10–12]). Not sensing the complexity of the initial dynamic behavior of exoelectrogens was the main deficiency of all the MFC model approaches. The necessity of understanding the mechanisms of the suspended microorganisms' distribution in anolyte and/or their attachment to anode surface to extend the biofilm, in dynamical modeling of MFCs is inevitable.

Picioreanu et al. [7] implemented MFC modeling based on the electron transfer mechanism of electron shuttles. In addition, the simulation of biofilm and anolyte was investigated in this study. In contrast, Kato Marcus et al. considered the electron transfer mechanism by nanowires of exolectrogenic microorganisms and modeled the MFC operation utilizing pure culture [9]. In latter studies, the model of Kato Marcus et al. was extended by considering complex wastewater and mixed culture and different kinetics of biochemical reactions [8,11]. Karimi et al. investigated the hierarchical biochemical processes of complex substrate degradation by different microorganisms [10–12]. The simulation of extracellular polymer substance (EPS) and the competition among different microorganism groups, particularly electrogen and methanogen, were the most significant part of their results. It should be noted that the modeling of bioelectrochemical system was implemented by engaging multiple-populations and complex substrates by Pinto et al. [13], but the essential difference between this study and those of Karimi et al. [10–12] is the electron transfer mechanisms by exoelectrogens.

In addition to the modeling of biocatalysts behaviors, the investigation of the kinetics of anodic and cathodic reactions [14], surface phenomena in electrodes [15], mass transfer in the interphase of anolyte and biofilm [16], biodegradation of different substrates [17] and the change in hydrodynamical conditions of systems [18] were considered in previous theoretical studies. The contemplation of the theoretical investigations of bioelectrochemical systems reveals that some of the subjects, as portrayed in Fig. 1, were studied in previous models.

With respect to the critical role of microorganism's behavior and to the best of our knowledge, there has been no theoretical investigation that focuses on the dynamical analysis of microorganisms from the random movement to biofilm formation in bioelectrochemical systems. The main deficiency of MFC models concerning spatial distribution of biocatalysts was to assume an initial distribution of attached/suspended bacteria on electrode or in anolyte bulk, which was the foundation for biofilm formation [9–13,19]. The obscurities such as the basis of random or directional movement of bacteria in anolyte bulk, the driving force of biofilm formation, and the main factors that affected initial bacterial distribution have not been addressed in previous modeling studies.

In present study, the quantitative data of bacteria chemotaxis was used to improve the performance of previous models as well as

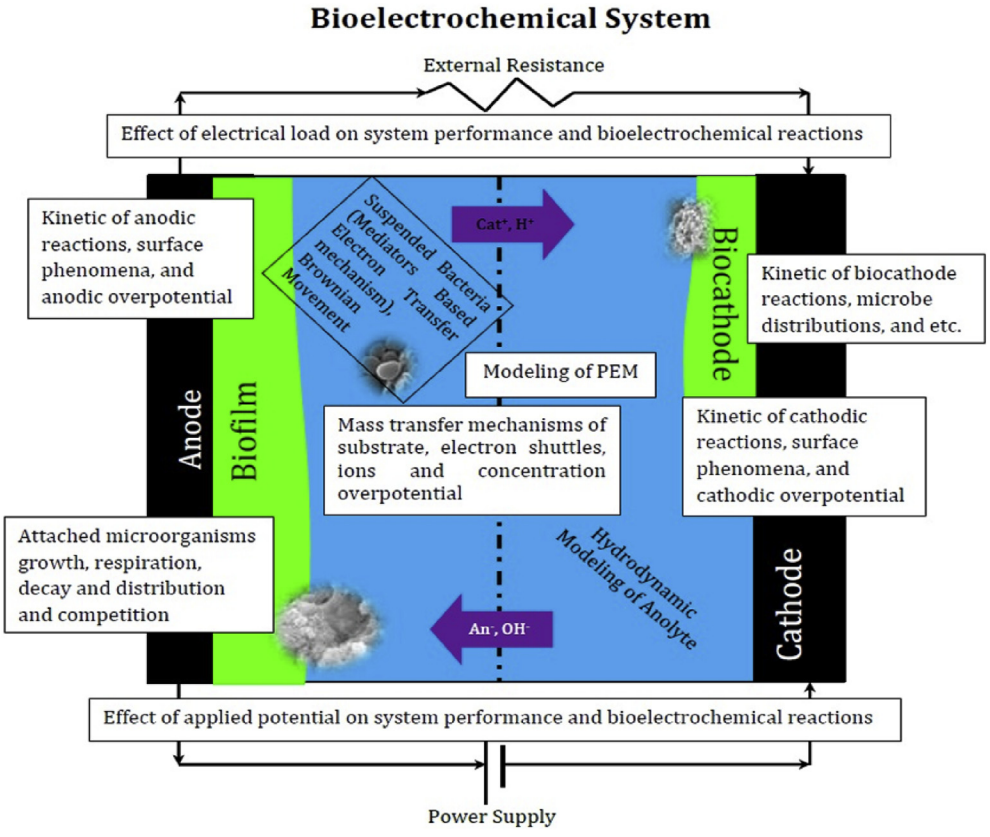

Fig. 1. Subjects of theoretical investigation of bioelectrochemical systems.

understand the mechanisms of the suspended microorganisms' distribution in anolyte and/or their attachment to anode surface. The presented model can be applied in a general manner to concern both electrons transfer mechanisms (including mediator based and conduction based) and the produced current of microfluidic MFC is calculated as a consequence of substrate bio-oxidation by both attached and suspended species. To the best of the authors' knowledge, besides the current work's prominent feature of investigating microbial population dynamics through novel chemotaxis assays, it is the first study of microfluidic MFC modeling. The performance of the microfluidic MFC as a chemotaxis assay was characterized on the basis of bacterial transport parameters.

3. Materials and methods

3.1. Experimental setup of microfluidic MFC

Microfluidic MFC was fabricated from poly methyl methacrylate (PMMA) plates as the main body consisting of a microchannel (7 cm in length; 1 mm in width; 1 mm in depth), a nickel plate anode, and carbon cloth cathode as previously described [20]. The carbon cloth cathode (5 cm in length and 3 mm in width) was fabricated as described by Cheng et al. [21] to result in 0.5 mg cm^{-2} of platinum loading and glued to one side of microchannel. A nickel plate anode (0.5 mm in thickness; 1 mm in width; 5 cm in length) was placed in front of the carbon cloth cathode that electrode spacing was equal to microchannel depth (i.e. 1 mm). The setup was operated at 25 °C. The microbial enrichment of the experimental setup of presented microfluidic MFC was achieved with *Escherichia coli*. *Escherichia coli* ATCC-11105 were obtained from the Biochemical and Bio-environmental Engineering Center of Sharif University of Technology and cultured in the nutrient broth (NB) medium (1 g l^{-1} beef extract, 2 g l^{-1} yeast extract, 5 g l^{-1} peptone, and 5 g l^{-1} NaCl) under anaerobic conditions at 37 °C [20].

The microfluidic MFC potential (V) was recorded automatically at 1 min intervals using a data logger connected to a personal computer. The external resistance (1–100 kΩ) of the cell was reduced stepwise to polarize the microfluidic MFC and monitor potential variation to produce polarization data. Microfluidic MFC characteristics of current (I) and power (P) were normalized to microchannel volume.

3.2. Model configuration

The current study was directed towards a mathematical description of the various biochemical processes from substrate biodegradation and bacterial distribution in anolyte by chemotaxis equations to electron generation in microfluidic MFC. Both the suspended bacteria in the anolyte and the attached ones in the biofilm were important considerations for the theoretical part of the present study. The biochemical equations of the system are presented in Sections 3.2.1 to 3.2.6. Later, the present model is verified with the experimental data of fabricated microfluidic MFCs in the current and other studies as well.

3.2.1. Substrate degradation rate

Organic substrate transformation to acetate by the fermentative microorganisms is assumed to occur in a single step:

$$Su\ (Substrate) \rightarrow aAc(Acetate) \tag{1}$$

where *Su* is the concentration of organic substrate, *Ac* is the acetate concentration, and *a* is the stoichiometric coefficient.

Based on the electron transfer mechanisms of suspended exoelectrogenic microorganisms via self-produced electron transfer mediators the following equation can be written for the acetate consumption [13]:

$$C_2H_4O_2 + 2H_2O + 4M_{ox} \rightarrow 4M_{red} + 2CO_2 \tag{2}$$

$$4M_{red} \rightarrow 4M_{ox} + 8e^- + 8H^+ \tag{3}$$

$$4e^- + 4H^+ + O_2 \rightarrow 2H_2O \tag{4}$$

According to Eq. (2), the acetate consumption and electron production take place through electrogens that convert the oxidized form of electron shuttles (M_{ox}) to reduced form (M_{red}). Furthermore, electrons are conducted to the cathode through an external circuit and protons are transferred to the cathode through a proton exchange membrane (PEM), and are reduced to water molecules in the presence of oxygen (Eq. (4)). The substrate consumption rate in anolyte of microfluidic MFC corresponding to suspended bacteria is described in Eq. (5) [13]:

$$q_{s,bulk} = q_{s,max}\psi_s\left(\frac{S_{d,bulk}}{S_{d,bulk}+K_{Sd}}\right)\left(\frac{M_{ox}}{M_{ox}+K_M}\right) \tag{5}$$

where $q_{s,bulk}$ and $q_{s,max}$ show the consumption rate ($kg_{CODS}\ m^{-3}\ day^{-1}$), and maximum consumption rate ($kg_{CODS}\ kg_{CODX}^{-1}\ day^{-1}$) of organic substrate by electrogenic bacteria in the anolyte bulk, respectively; $S_{d,bulk}$ ($kg_{CODS}\ m^{-3}$) and M_{ox} ($kg_{mediator}\ kg_{CODX}^{-1}$) are the substrate concentration and oxidized electron shuttles fraction in liquid bulk, respectively; ψ_s donates suspended bacteria concentration ($kg_{CODx}^{-1}\ m^{-3}$) and K_M is oxidized electron shuttles consumed and produced by suspended bacteria ($kg_{mediator}\ kg_{CODX}^{-1}$).

For the attached microorganisms corresponding to conduction-based electron transfer mechanisms, the substrate consumption rate in biofilm of microfluidic MFC is described in Eq. (6) [9]:

$$q_{s,biofilm} = q_{s,max}\psi_a\left(\frac{S_d}{S_d+K_{Sd}}\right)\left(\frac{1}{1+\exp\left(-\frac{F}{RT}\eta\right)}\right) \tag{6}$$

where $q_{s,biofilm}$ and $q_{s,max}$ show the consumption rate ($kg_{CODS}\ m^{-3}\ day^{-1}$), and maximum consumption rate ($kg_{CODS}\ kg_{CODX}^{-1}\ day^{-1}$) of organic substrate in the biofilm, respectively. S_d represents substrate concentration in biofilm ($kg_{CODS}\ m^{-3}$); ψ_a donates attached bacteria concentration ($kg_{CODx}^{-1}\ m^{-3}$); η is local potential of anode surface (V); F is Faraday's constant (96485 C mol−e $^{-1}$); R donates the universal gas constant (8.314 J $mol^{-1}\ K^{-1}$) and T represents the anolyte temperature (K).

3.2.2. Substrate concentration distributions

The substrate diffusion is the dominant transport mechanism of mass transfer into the porous solid biofilm and determined by Eq. (7):

$$D_{s,f}\frac{\partial^2 S_d}{\partial z^2} - q_{s,biofilm} = 0 \tag{7}$$

$D_{s,f}$ is the diffusion coefficient of substrate in the biofilm ($m^2\ day^{-1}$), and z shows the spatial longitudinal coordinate from the anode surface (m).

As there is no substrate flux on the anode surface, and there is an interphase mass transfer at the biofilm/liquid bulk interface, the boundary conditions of the above equation can be described in Eq. (8) and Eq. (9):

$$\frac{\partial S_d}{\partial z}\Big|_{z=0} = 0 \tag{8}$$

$$D_{s,f}\frac{dS_d}{dz}\Big|_{z=L_f} = \left(\frac{D_{s,l}}{l}\right)\left(S_{d,bulk} - S_{d,surface}\right) \tag{9}$$

where l and $S_{d,surface}$ donate the thickness of liquid concentration boundary layer (m) and substrate concentration at the liquid bulk/biofilm interface ($kg_{CODS}\ m^{-3}$), respectively. $D_{s,f}$ and $D_{s,l}$ represent substrate diffusion coefficient in the porous biofilm and anolyte bulk ($m^2\ day^{-1}$), respectively.

The variation of substrate concentration in anolyte is described through Eq. (10):

$$\frac{\partial S_{d,bulk}}{\partial t} = D(S_{d,in} - S_{d,bulk}) - q_{s,bulk} - \left(\frac{A_{an}}{V_{micro}}\right)J_{biofilm} \tag{10}$$

The first step of Eq. (10) is the temporal variation of substrate concentration. This is equal to the substrate convection in the bulk solution minus degradation rate of substrate by suspended microorganisms and substrate diffusion to biofilm. D (day^{-1}) represents dilution rate of microfluidic MFC and is equal to the proportion of substrate flow rate to anolyte volume; A_{an} is the anode surface area (m^2) and $J_{biofilm}$ represents the substrate flux from anolyte into biofilm ($kg_{CODS}\ m^{-2}\ day^{-1}$).

The initial condition for Eq. (10) can be satisfied by the substrate concentration in the inlet of microfluidic MFC (Eq. (11)):

$$S_{d,bulk}|_{t=0} = S^0_{d,bulk} \tag{11}$$

where $S^0_{d,bulk}$ is substrate concentration in the microchannel inlet ($kg_{CODS}\ m^{-2}$).

3.2.3. Electron mass balance equations

The production of electrons from suspended bacteria and electron transfer through anolyte by electron shuttles is illustrated by the mediator mass balance equation in the anolyte of microfluidic MFC:

$$M_{Total} = M_{red} + M_{ox} \tag{12}$$

where M_{Total}, M_{red} and M_{ox} represent total, reduced and oxidized mediators fraction per total mass of suspended electrogenic microorganisms ($kg_{mediator}\ kg^{-1}_{CODX}$). As mentioned, by substrate consumption, the electron production is initiated by electrogens and converted the oxidized form of electron shuttles (M_{ox}) to reduced form (M_{red}). The mass balance of oxidized mediators is written as:

$$\frac{dM_{ox}}{dt} = -\gamma_M q_{s,max} + \frac{M_{Med} \times I_{MFC} \times 86.4}{V_{micro} \times \psi_s \times nF} \tag{13}$$

In Eq. (13) the temporal variation of oxidized form of mediators is equal to summation of mediator generation due to substrate consumption by bacteria and reduction of oxidized form of mediator which is illustrated by produced current in microfluidic MFC ($I_{MFC}/A\ m^{-3}$). γ_M is the oxidized mediator yield ($kg_{mediator}\ kg^{-1}_{CODS}$); M_{Med} represents the mediator molecular weight ($kg_{mediator}\ kmole^{-1}_{mediator}$) and n donates the number of electrons transferred per mole of mediator ($kmole_{electrons}\ kmole^{-1}_{mediators}$).

Microfluidic MFC potential (E_{Actual}) can be calculated using theoretical cell potential ($E_{Theoretical}$) by subtracting activation (η_{Act}), ohmic (η_{Ohm}), and concentration (η_{Con}) overpotentials. Therefore, the following relation can be written as:

$$E_{Actual} = E_{Theoretical} - \eta_{Act} - \eta_{Ohm} - \eta_{Con} \tag{14}$$

As has been discussed in previously published results [13], the overpotentials were described with following relations:

$$\eta_{Act} = \frac{RT}{\delta nF}\sinh^{-1}\left(\frac{I_{MFC}}{A_{an} i_0}\right) \tag{15}$$

$$\eta_{Ohm} = I_{MFC} R_{ohm} \tag{16}$$

$$\eta_{Con} = \frac{RT}{nF}\ln\left(\frac{M_{Total}}{M_{red}}\right) \tag{17}$$

where i_0 represents the exchange current density in reference conditions ($A\ m^{-2}$); δ is either the reduction or the oxidation transfer coefficient (dimensionless), and R_{ohm} donates the ohmic resistance of microfluidic MFC (Ω) and can be calculated using the anolyte conductivity:

$$R_{Ohm} = \frac{H_{micro}}{k_{sol} A_{an}} \tag{18}$$

where k_{sol} represents the anolyte conductivity ($S\ m^{-1}$). H_{micro} (m) denotes the height of microchannel. By substituting E_{Actual} by IR_{ext} and simplifying the relation, the produced current of suspended microorganism's activity is calculated from Eq. (19):

$$I_{MFC} = \frac{1}{R_{ext}}\left(E_{Theoretical} - \frac{RT}{\delta nF}\sinh^{-1}\left(\frac{I_{MFC}}{A_{an} i_0}\right) - I_{MFC} R_{ohm} - \frac{RT}{nF}\ln\left(\frac{M_{Total}}{M_{red}}\right)\right) \tag{19}$$

The calculation of produced current density in Eq. (19), donates the rate of produced electrons that transferred by self-produced electron shuttles.

The conduction of electrons through biofilm via nanowires, in response to the electric field, is described by Ohm's law (Eq. (20)):

$$j = -\kappa_{bio}\frac{d\eta}{dz} \tag{20}$$

where j and κ_{bio} are the current density ($A\ m^{-2}$) and the biofilm conductivity ($S\ m^{-1}$), respectively. The electron mass balance equation in the biofilm is presented by Eq. (21) [9]:

$$\kappa_{bio}\frac{d^2\eta}{dz^2} - \frac{F\gamma_1}{\tau} f_e^0\, q_{s,biofilm} - \frac{F\gamma_2}{\tau}\ r_{res} = 0 \tag{21}$$

γ_1 (mole electron kg^{-1}_{CODS}) and γ_2 (mole electron kg^{-1}_{CODX}) are the electrons generated by substrate consumption and the endogenous respiration, respectively; r_{res} is endogenous respiration rate of bacteria in biofilm ($kg_{CODX}\ m^{-3}\ day^{-1}$); f_e^0 represents the fraction of energy-generating electrons (dimensionless) and τ donates time conversion factor ($86400\ s\ day^{-1}$).

The endogenous respiration kinetics is utilized as electron production rate from bacterial self-oxidation [9]:

$$r_{res} = b_{res}\psi_a\left(\frac{1}{1+\exp\left(\frac{-F}{RT}\eta\right)}\right) \tag{22}$$

where b_{res} donates the respiration constant (day^1).

As has been discussed in our previously published studies [10–12], the boundary conditions of Eq. (21) can be characterized based on the bioanode potential status. At the interface of the anolyte and biofilm ($z = L_f$) the electron flux of suspended bacteria should be considered. Therefore, the first boundary condition is written as follows:

$$\left.\frac{d\eta}{dz}\right|_{z=L_f} = \frac{1}{-\kappa_{bio}} I_{MFC} H_{micro} \tag{23}$$

In addition, the relationships among the cell potential, current and relative local biofilm potential were combined to acquire the second boundary condition as Eq. (24) [10]:

$$\eta|_{z=0} - (A_{an} \cdot \kappa_{bio} \cdot (R_{ext} + R_{int})) \left.\frac{d\eta}{dz}\right|_{z=0} = V_{cat} - E_{KA} \tag{24}$$

where V_{cat} shows actual cathode potential (V). R_{int}, R_{ext}, E_{KA} donate internal resistance (Ω), external resistance (Ω), and the half maximum rate potential (V), respectively. This boundary condition (i.e. Eq. (24)) can be used to simulate the polarization characteristics of a microfluidic MFC. Eventually, for a poised anode surface potential Eq. (25) is applied instead of the variable boundary condition (i.e. Eq. (24)) [12]:

$$\eta_{z=0} = V_{anode} - E_{KA} \tag{25}$$

3.2.4. Bacteria distribution in microfluidic MFC

Based on Brownian motions of bacteria and interaction between electrode surface and microorganisms [22,23], the adhesion of bacteria was initiated in the form of biofilm which would be thicker by EPS secretion [24,25]. As mentioned, the presence of the stimulus suppresses tumbling and leads to biasing of the random walk allowing the bacteria to accumulate in environments containing high attractant concentrations.

Bacteria produce sensing molecules as they move through the bulk of the fluid. The sensing molecules radically diffuse away from the suspended bacteria and get reflected once those molecules reach the electrodes surface. The bacteria sense their proximity to the electrodes surface and keep moving toward the nearest surface where they adsorb, resulting in more sensing molecules produced at the boundaries. This increased production intensifies the recruitment of bacteria to the pioneering colonies, which will merge to form the biofilm [26]. To predict the direction of bacteria movement, the mass balance of sensing molecules can be described as follows:

$$\frac{\partial S_E}{\partial t} = D_E \frac{\partial^2 S_E}{\partial z^2} - \lambda S_E + \alpha \psi_s \tag{26}$$

where S_E (kg_{CODS} m^{-3}) is the sensing molecules concentration at spatial position z and time t; D_E is the diffusion coefficient of the secreted sensing molecules (m^2 day^{-1}); λ is sensing molecules degradation rate (day^{-1}) and α is sensing molecules production rate in the free-space (kg_{CODS} kg_{CODX}^{-1} day^{-1}).

The initial and boundary conditions of Eq. (26) are written as initial concentration of sensing molecules in anolyte and the flux of secreted sensing molecules in boundaries of biofilm:

$$S_E|_{t=0} = S_{E_0} \tag{27}$$

$$D_E \left.\frac{\partial S_E}{\partial z}\right|_{z=L_f} = \omega \psi_a \tag{28}$$

$$\left.\frac{\partial S_E}{\partial z}\right|_{z=H_{micro}} = 0 \tag{29}$$

where S_{E0} is initial concentration of sensing molecules in anolyte (kg_{CODS} m^{-3}); ω represents sensing molecules production rate in the boundaries (m kg_{CODS} kg_{CODX}^{-1} day^{-1}).

For initial bacterial distribution in the anolyte of microfluidic MFC based on the swimming of bacteria toward the concentration bands of secreted sensing molecules the following equation has been presented [26]:

$$\frac{\partial \psi_s}{\partial t} = \mu_{SE0} \frac{\partial^2 \psi_s}{\partial z^2} - \chi_{s0} \frac{\partial}{\partial z}\left(\psi_s \frac{\partial S_E}{\partial z}\right) + \gamma q_{s,bulk} - r_{ina,bulk} \tag{30}$$

where μ_{SE0} (m^2 day^{-1}) and χ_{s0} (m^5 kg_{CODX}^{-1} day^{-1}) are the random motility coefficients of sensing molecules and chemotactic coefficients of sensing molecules, respectively. γ (kg_{CODX} kg_{CODS}^{-1}) is the microbial yields of bacteria and $r_{ina,bulk}$ (kg_{CODX} m^{-3} day^{-1}) represents the inactivation rate of suspended bacteria and can be described by first-order kinetics in respect to the active bacteria concentrations, as shown in Eq. (31) [27]:

$$r_{ina,bulk} = b_{ina} \psi_s \tag{31}$$

b_{ina} donates the inactivation constant (day^{-1}).

On the right hand side of Eq. (30), the first term represents the bacteria diffusion in the anolyte which frees the concentration gradient of sensing molecules. The second term, on the other hand, describes the bacterial movement as a function of concentration gradient of sensing molecules.

The suspended bacteria cannot permeate through the membrane of microfluidic MFC. In addition, there is zero concentration of suspended bacteria at the surface of electrodes. Therefore, the required boundary conditions for Eq. (30) are as follows:

$$\psi_s|_{z=0} = 0 \tag{32}$$

$$\left.\frac{\partial \psi_s}{\partial z}\right|_{z=H_{micro}} = 0 \tag{33}$$

Finally, the initial condition of Eq. (30) is characterized as initial concentration of suspended bacteria in the inlet of microchannel:

$$\psi s|_{t=0} = \psi_{s0} \tag{34}$$

The bacterial flux on the electrodes surface for biofilm formation can be described by a generalized Keller–Segel (K–S) model of the form [28,29]:

$$\frac{\partial \psi_a}{\partial t} = \mu \frac{\partial^2 \psi_a}{\partial z^2} - \frac{\partial}{\partial z}(V \psi_a) + \textit{Bacteria Growth} - \textit{Bacteria Dead} - \textit{Bacteria Respiration} \tag{35}$$

where ψ_a represents the concentration of attached bacteria (kg_{CODX} m^{-3}); V (m day^{-1}) is the chemotactic velocity and μ donates random motility of bacteria (m^2 day^{-1}). Both random motility and chemotactic velocity are functions of the attractant concentration [30]. Rivero et al. [31] derived the following expressions for the random motility and chemotactic velocity, in terms of the single-cell properties. These expressions were modified by Ahmed and Stocker for one dimensional velocity of single cell [3]:

$$V = \vartheta \tanh\left(\frac{\chi_0}{\vartheta} \frac{K_D}{(K_D + S_{d,bulk})^2} \frac{\partial S_{d,bulk}}{\partial z}\right) \tag{36}$$

$$\mu = \frac{\vartheta^2}{(1-\varphi)p_0}\exp\left(\frac{\chi_0}{\vartheta^2}\frac{K_D}{\left(K_D+S_{d,bulk}\right)^2}\frac{\partial S_{d,bulk}}{\partial t}\right) \times \operatorname{sech}\left(\frac{\chi_0}{\vartheta}\frac{K_D}{\left(K_D+S_{d,bulk}\right)^2}\frac{\partial S_{d,bulk}}{\partial z}\right) \quad (37)$$

$$\mu_{s0} = \frac{\vartheta^2}{(1-\varphi)p_0} \quad (38)$$

where ϑ is the swimming speed of an individual bacterium (m day^{-1}); μ_{s0} represents random motility coefficient of bacteria (m^2 day^{-1}) (analogous to a molecular diffusion coefficient); φ is direction persistence (dimensionless), p_0 is individual bacterial tumbling probability in the absence of a chemoattractant gradient (day^{-1}), χ_0 donates chemotactic sensitivity coefficient of substrate (m^2 day^{-1}); $S_{d,bulk}$ is the substrate concentrations in liquid bulk (kg$_{CODS}$ m^{-3}) and K_D represents the receptor ligand dissociation constant as function of interaction between the substrate and cell membrane of microorganisms (kg$_{CODS}$ m^{-3}).

There is a continuous condition of experimental setup of microfluidic MFC and no variation of substrate concentration versus time. Thus, the exponential term of Eq. (37) is eliminated and random motility coefficient is simplified as:

$$\mu = \mu_{s0}\operatorname{sech}\left(\frac{\chi_0}{\vartheta}\frac{K_D}{\left(K_D+S_{d,bulk}\right)^2}\frac{\partial S_{d,bulk}}{\partial z}\right) \quad (39)$$

The bacterial growth on the electrodes surface as well as bacteria coming from free-space and getting stuck on the electrodes surface is included in Eq. (35):

$$Bacteria\ growth = SR(t) + \gamma q_{s,biofilm} \quad (40)$$

where $SR(t)$ represents stickiness rate of suspended bacteria (kg$_{CODX}$ m^{-3} day^{-1}) and $\gamma q_{s,biofilm}$ are bacterial growth on the electrode surface as a function of substrate consumption. $q_{s,biofilm}$ is the consumption rate of substrate by attached bacteria (kg$_{CODS}$ m^{-3} day^{-1}).

The relationship between stuck-bacteria at the surface at each time t and the suspended bacteria concentration is written as [32]:

$$SR(t) = \beta\left(\mu_{s0}\frac{\partial\psi_s}{\partial z}\bigg|_{z=0}\right) \quad (41)$$

β represents bacterial stickiness coefficient (m^{-1}).

Similar to suspended bacteria, the inactivation rate of attached bacteria represents by Eq. (42) [27]:

$$r_{ina,biofilm} = b_{ina}\psi_a \quad (42)$$

where $r_{ina,biofilm}$ donates inactivation rate of attached microorganisms (kg$_{CODX}$ m^{-3} day^{-1}) and b_{ina} represents the inactivation constant (day^{-1}).

Finally, the expanded form of a generalized Keller–Segel (K–S) model for bacteria distribution in biofilm is written as (Eq. (43)):

$$\frac{\partial\psi_a}{\partial t} = \left(\left[\mu_{s0}\operatorname{sech}\left(\frac{\chi_0}{\vartheta}\frac{K_D}{\left(K_D+S_{d,bulk}\right)^2}\frac{\partial S_{d,bulk}}{\partial z}\right)\right]\frac{\partial^2\psi_a}{\partial z^2}\right) - \frac{\partial}{\partial z}\left(\left[\vartheta\tanh\left(\frac{\chi_0}{\vartheta}\frac{K_D}{\left(K_D+S_{d,bulk}\right)^2}\frac{\partial S_{d,bulk}}{\partial z}\right)\right]_a\psi_a\right) + \beta\left(\mu_{s0}\frac{\partial\psi_s}{\partial z}\bigg|_{z=0}\right) + \gamma q_{s,biofilm} - r_{ina,biofilm} - r_{res} \quad (43)$$

At the anode surface (z = 0) and at the interface of the anolyte and biofilm (z = L$_f$), there is no mass flux for bacteria because of the low thickness of biofilm in microfluidic MFC. This leads to low probability of biofilm detachment, and no interphase mass flux between attached and suspended bacteria is considered. Therefore, the boundary conditions are as follows:

$$\frac{\partial\psi_a}{\partial z}\bigg|_{z=0} \quad (44)$$

$$\frac{\partial\psi_a}{\partial z}\bigg|_{z=L_f} = 0 \quad (45)$$

The initial condition for Eq. (20) was considered as the first layer thickness of the bacteria concentration attached in the first step. This is equal to the thickness of one bacteria:

$$\psi_a|_{t=0} = (Equivalent\ to\ the\ thickness\ of\ one\ bacteria) \quad (46)$$

3.2.5. Biofilm thickness

Changes in the biofilm thickness is evaluated by the net biomass growth on the electrode surface and disengagement of microorganisms from the biofilm, recognized as the detachment phenomenon [12]. As mentioned, detachment of biofilm is expected in high thickness of biofilm and unavailability of nutrient [33]. In microfluidic MFC, because of the low thickness of biofilm, controllable feed injections in the experimental setup and accessibility of microorganisms to sufficient nutrient, the detachment of microorganisms is considered negligible.

The individual model and mass balance for biofilm formation depend on the behavior of biomass particles. These particles grow by the uptake of nutrients, producing and excreting metabolites such as EPS, and dividing once a critical size is reached. The particles produce an offspring biomass element in spherical compartments, with variable composition and location, in space and where biochemical reactions take place. The mass of each particulate species that is part of the composition of a biomass particle changes in time according to the following equation [34]:

$$\frac{dM_n}{dt} = M_n\gamma q_{s,max}\left(\frac{S_{d,bulk}}{S_{d,bulk}+K_{Sd}}\right) + M_n b_{ina} + M_n b_{res} \quad (47)$$

where M_n represents the mass of biomass particles (kg$_{CODX}$) and K_{Sd} represents the Monod half-saturation constants of substrate (kg$_{CODS}$ m^{-3}). By assuming the constant density of microorganisms Eq. (47) is presented with respect to spherical biomass particles growth:

$$\frac{d}{dt}\left(X_a\left(\frac{4}{3}\pi r_n^3\right)\right) = \left(X_a\left(\frac{4}{3}\pi r_n^3\right)\left[\gamma q_{s,max}\left(\frac{S_{d,bulk}}{S_{d,bulk}+K_{Sd}}\right) + b_{ina} + b_{res}\right]\right) \tag{48}$$

where r_n represent the biomass particles radius (m) and X_a the density of biomass particles ($kg_{CODX}\ m^{-3}$). Eq. (48) shows that the changes in the biofilm thickness are eventuated by summation of the following elements: advective growth of attached bacteria as biomass particles, the thickness of inactivated bacteria, and the thickness of suspended bacteria coming from the free-space and getting stuck on the electrodes surface:

$$L_f = L_{f0}\sqrt[3]{\exp\left(\left[\gamma q_{s,max}\left(\frac{S_{d,bulk}}{S_{d,bulk}+K_{Sd}}\right) + b_{ina} + b_{res}\right]t\right)} + \left(T_{f(stickiness)}t\right) \tag{49}$$

where L_{f0} represents the thickness of individual bacterium cell (m). The rate of suspended bacteria coming from the free-space and stuck on the electrodes surface is described in Eq. (50):

$$T_{f(stickiness)} = \frac{SR(t)\times V_{micro}}{X_a \times A_{an}} = \frac{\beta\left(\mu_{s0}\frac{\partial\psi_s}{\partial z}\Big|_{z=0}\right)\times H_{micro}}{X_a} \tag{50}$$

where $T_{f(stickiness)}$ denotes the rate of suspended bacteria coming from the free-space and stuck on the electrodes surface (m day^{-1}); A_{an} represents the surface area of the anode (m^2) and V_{micro} (m^{-3}) denotes the volume of microchannel.

3.2.6. Numerical analysis

To simplify parameters and eliminate variables dimensions, all variables used in the above equations were normalized as follows:

$$z^* = \frac{z\vartheta}{D_{s,f}} \tag{51}$$

$$t^* = \frac{t\vartheta^2}{D_{s,l}} \tag{52}$$

$$S_d^* = \frac{S_d}{K_{sd}} \tag{53}$$

$$S_{d,bulk}^* = \frac{S_{d,bulk}}{K_{Sd}} \tag{54}$$

$$S_E^* = \frac{S_E}{S_{E0}} \tag{55}$$

$$M_{ox}^* = \frac{M_{ox}}{K_M} \tag{56}$$

$$q_{s,biofilm}^* = \frac{q_{s,\ biofilm}}{q_{s,max}\psi_a} \tag{57}$$

$$q_{s,bulk}^* = \frac{q_{s,bulk}}{q_{s,max}\psi_s} \tag{58}$$

$$r_{ina,biofilm}^* = \frac{r_{ina,biofilm}}{b_{ina,\ biofilm}\psi_a} \tag{59}$$

$$r_{ina,bulk}^* = \frac{r_{ina,bulk}}{b_{ina,\ bulk}\psi_s} \tag{60}$$

$$\psi_a^* = \frac{\psi_a}{X_a} \tag{61}$$

$$\psi_s^* = \frac{\psi_s}{\psi_{s0}} \tag{62}$$

$$\eta^* = \frac{\eta}{V_{cat}} \tag{63}$$

$$I^* = \frac{I}{\frac{V_{cat}}{R_{int}}} \tag{64}$$

$$L_f^* = \frac{L_f}{H_{micro}} \tag{65}$$

$$r_{res}^* = \frac{r_{res}}{b_{res}\psi_a} \tag{66}$$

The dimensionless form of presented equations is listed as follow:

$$q_{s,bulk}^* = \left(\frac{S_{d,bulk}^*}{S_{d,bulk}^*+1}\right)\left(\frac{M_{ox}^*}{M_{ox}^*+1}\right) \tag{67}$$

$$q_{s,biofilm}^* = \left(\frac{S_d^*}{S_d^*+1}\right)\left(\frac{1}{1+\exp\left(-\frac{FV_{cat}}{RT}\eta^*\right)}\right) \tag{68}$$

$$\frac{\partial S_E^*}{\partial t^*} = D_E\left(\frac{D_{s,l}}{D_{s,f}}\right)^2\frac{\partial^2 S_E^*}{\partial z^{*2}} - \left(\frac{D_{s,l}}{\vartheta}\right)^2\lambda\left(S_E^*\right) + \left(\frac{D_{s,l}}{\vartheta}\right)^2\left(\frac{\psi_{s0}\alpha}{S_{E0}}\right)\left(\psi_s^*\right) \tag{69}$$

$$\frac{\partial^2 S_d^*}{\partial z^{*2}} - q_{s,biofilm}^*\psi_a^*\left(\frac{X_a q_{s,\ max} D_{s,f}}{K_{Sd}\vartheta^2}\right) = 0 \tag{70}$$

$$\frac{\partial S_{d,bulk}^*}{\partial t^*} = D\frac{D_{s,l}}{\vartheta^2}\left(S_{d,in}^* - S_{d,bulk}^*\right) - \left(\frac{D_{s,l}q_{s,max}\psi_{s0}}{\vartheta^2 K_{Sd}}\right)\left(\psi_s^* q_{s,bulk}^*\right) - \left(\frac{D_{s,l}A_{an}}{\vartheta^2 K_{Sd}V_{anolyte}}\right)J_{biofilm} \tag{71}$$

$$\frac{dM_{ox}^*}{dt^*} = -\left(\frac{\gamma_M q_{s,max}D_{s,l}}{K_M\vartheta^2}\right) + \left(\frac{M_{Med}D_{s,l}V_{Cat}\times 86.4}{K_M\vartheta^2\psi_{s0}V_{micro}\times R_{int}\times nF}\right)\times\left(\frac{I_{MFC}^*}{\psi_s^*}\right) \tag{72}$$

$$\frac{\partial \psi_s^*}{\partial t^*} = \left(\frac{\mu_{SE0} D_{s,l}}{D_{s,f}^2}\right) \frac{\partial^2 \psi_s^*}{\partial z^{*2}} - \left(\frac{D_{s,l}\chi_{s0} S_{E0}}{D_{s,f}^2}\right) \frac{\partial}{\partial z^*}\left(\psi_s^* \frac{\partial S_E^*}{\partial z^*}\right) + \left(\frac{D_{s,l} q_{s,max}\gamma}{\vartheta^2}\right)\left(q_{s,bulk}^* \psi_s^*\right) - \left(\frac{D_{s,l} b_{ina,bulk}}{\vartheta^2}\right)\psi_s^* r_{ina,bulk}^* \tag{73}$$

$$\frac{\partial \psi_a^*}{\partial t^*} = \frac{\mu_{s0} D_{s,l}}{D_{s,f}^2}\left(\left[\operatorname{sech}\left(\left(\frac{K_{Sd}\chi_0}{D_{s,f}}\right)\frac{1}{\left(1+\frac{S_{d,bulk}^* K_{Sd}}{K_D}\right)^2}\frac{\partial S_{d,bulk}^*}{\partial z^*}\right)\right]\frac{\partial^2 \psi_a^*}{\partial z^{*2}}\right) - \left(\frac{D_{s,l}}{D_{s,f}}\right)\frac{\partial}{\partial z^*}\left(\left[\tanh\left(\left(\frac{K_{Sd}\chi_0}{K_D D_{s,f}}\right)\frac{1}{\left(1+\frac{S_{d,bulk}^* K_{Sd}}{K_D}\right)^2}\frac{\partial S_{d,bulk}^*}{\partial z^*}\right)\right]\left(\psi_a^*\right)\right) + \left(\frac{\beta \psi_{s0}\mu_{s0} D_{s,l}}{\vartheta X_a D_{s,f}}\right)\left(\left.\frac{\partial \psi_s^*}{\partial z^*}\right|_{z=0}\right) + \left(\frac{D_{s,l}\gamma q_{s,max}}{\vartheta^2}\right)\left(q_{s,biofilm}^* \psi_a^*\right) - \left(\frac{D_{s,l} b_{ina}}{\vartheta^2}\right)\psi_a^* r_{ina,biofilm}^* - \left(\frac{D_{s,l} b_{res}}{\vartheta^2}\right)\psi_a^* r_{res}^* \tag{74}$$

$$\frac{d^2\eta^*}{dz^{*2}} - \left(\frac{D_{s,f}^2 F\,\gamma_1 f_e^0\, X_a q_{s,max}}{\kappa_{bio} V_{Cat}\tau\vartheta^2}\right)\left(q_{s,biofilm}^* \psi_a^*\right) - \left(\frac{D_{s,f}^2 F\,\gamma_2 X_a b_{res}}{\kappa_{bio} V_{Cat}\tau\vartheta^2}\right)\left(r_{res}^* \psi_a^*\right) = 0 \tag{75}$$

$$L_f^* = \frac{L_{f0}}{H_{micro}}\sqrt[3]{\exp\left(\left[\left(\gamma q_{s,max}\left(\frac{S_{d,bulk}^*}{S_{d,bulk}^*+1}\right)+b_{ina}+b_{res}\right)\left(\frac{D_{s,l}}{\vartheta^2}\right)\right]t^*\right) + \left(\frac{\beta\mu_{s0} D_{s,l}\psi_{s0}}{X_a D_{s,f}\vartheta}\right)\left(\left.\frac{\partial \psi_s^*}{\partial z^*}\right|_{z^*=0}\right)t^*} \tag{76}$$

The numerical method of the model is a sequential time-stepping solution to solve the nonlinear coupled system of several ordinary and partial differential equations. As a result of mesh independency study, a 50-node grid was implemented with a simulation time step of 0.001 a day for substrate and bacteria concentrations, bacteria distribution, and potential spatial distributions in the biofilm and substrate, and suspended bacteria concentration in anolyte bulk of the microfluidic MFC. All ordinary and partial differential equations mentioned in this model are discretized by the finite difference method and solved by the Trust-Region-Reflective method [35]. By using the recent values of substrate concentration, microorganism distributions in the microchannel and its electrical potential are solved by the backward implicit Euler method [36].

Table 1
Model parameters values for glucose fed microfluidic MFC simulation.

Parameter	Value/Unit	Ref	Parameter	Value/Unit	Ref
$q_{s,max}$	52.86 $kg_{CODS}\ kg_{CODX}^{-1}\ day^{-1}$	[37]	D_E	0.876 $cm^2\ day^{-1}$	[b]
$D_{s,l}(Glucose)$	0.596 $cm^2\ day^{-1}$	[38]	$D_{s,f}$ (*Glucose*)	0.485 $cm^2\ day^{-1}$	[39]
l[a]	0.001 cm	[b]	X_a	300 $kg_{CODX}\ m^{-3}$	[7]
S_{E0}	0.01 $kg_{CODS}\ m^{-3}$	[b]	ψ_{S0}	1.6 $kg_{CODX}\ m^{-3}$	[b]
K_{sd}	0.01 $kg_{CODS}\ m^{-3}$	[37]	K_D	0.32 $kg_{CODS}\ m^{-3}$	[3]
K_M	10^{-5} $kg_{mediator}\ kg_{CODX}^{-1}$	[13]	κ_{bio} (*E. coli*)	0.005 mS cm^{-1}	[40]
γ_1	125 mol-e kg_{CODS}^{-1}	[27]	γ_2	125 mole-e kg_{CODX}^{-1}	[27]
γ_M	31.38 $kg_{mediator}\ kg_{CODS}^{-1}$	[7]	γ	0.243 $kg_{CODX}\ kg_{CODS}^{-1}$	[7]
b_{ina}	0.02 day^{-1}	[27]	b_{res}	0.07 day^{-1}	[9]
μ_{SE0}	0.864 $cm^2\ day^{-1}$	[b]	μ_{s0} (*E. coli*)	1.296 $cm^2\ day^{-1}$	[30]
χ_{s0}	13 $cm^5\ kg_{CODX}^{-1}\ day^{-1}$	[b]	χ_0(*E. coli*)	86.4 $cm^2\ day^{-1}$	[3]
ω	5×10^{-5} m $kg_{CODS}\ kg_{CODX}^{-1}\ day^{-1}$	[b]	ϑ (*E. coli*)	20 μm s^{-1}	[41]
λ	0.002 day^{-1}	[b]	β	0.3 m^{-1}	[32]
α	0.001 $kg_{CODS}\ kg_{CODX}^{-1}\ day^{-1}$	[b]	i_0	1 A m^{-2}	[13]
M_{Med}	663.4 kg-mediator $kmole\text{-}mediator^{-1}$	[13]	M_{total}	0.05 kg-mediator $kgCOD_X^{-1}$	[13]
n	2 mole-e $mole_{mediators}^{-1}$	[13]	$V_{anod-med}$	0.477 V	[7]
L_{micro}	5 cm	[20]	H_{micro}	0.1 cm	[20]
V_{micro}	50 μl	[20]	A_{an}	0.5 cm^2	[20]
δ	0.5 Dimensionless	[13]	f_e^0	0.9 Dimensionless	[27]
E_{KA}	−0.45[a] vs. SHE/V	[10]	V_{cat}	0.25 vs. SHE/V	[42]
F	96485 Coulomb $gmole\text{-}e^{-1}$	[38]	R	8.314 J $gmol^{-1}\ K^{-1}$	[38]

[a] Diffusion layer thickness.
[b] Estimated based on similar studies.

4. Results and discussion

4.1. Model verification

The experimental results from glucose fed microfluidic MFC [20] were used for model validation. The model constants are presented in Table 1.

The model prediction results and the experimental data [20] are illustrated in Fig. 2. The validation of the power density curves of the presented model in different glucose injection rates showed that the model prediction and experimental data coincided appropriately.

Since the validation of experimental data and model predictions is a strong function of consistency of microorganism's concentration and distribution [12,13], the verification of the output results (Fig. 2) reveals that the significant configurations of the present model in view of electron transfer mechanisms as well as bacteria chemotaxis as the foundation of biofilm formation are compatible with real conditions.

4.2. Evaluation of microfluidic MFC characteristics

The evolution of spatial distribution of attached dimensionless concentration of bacteria and substrate in biofilm of microfluidic MFC are shown in Fig. 3a and b, respectively.

The trend of dimensionless concentration of attached bacteria as a function of microchannel height and operation time is ascending but the evolution of dimensionless bacteria concentration reaches a sustained state (about 0.6) after 17 h (Fig. 3a). This is attributed to the decay, endogenous respiration and detachment of biofilm that was investigated in the previous studies [10,11,43]. As it was shown in previous studies [12,44], the concentration of attached bacteria is increased by increasing the distance from anode that attributed to accessibility of nutrient in surface of biofilm which the net growth rate of these bacteria would be higher.

The temporal and spatial distribution of substrate concentration in biofilm is shown in Fig. 3b. The substrate concentration dropped abruptly after 8 h indicating a significant increase in the attached biofilm concentration (Fig. 3a). The decline of temporal distribution of substrate concentration decreased after 14 h, which is equivalent to a decrease of the attached bacteria growth rate. As it was shown in previous studies [12,44], an accessibility to the nutrient plays a key role in biofilm formation, which conforms to the ascending behavior of the spatial distribution of bacteria concentration (Fig. 3b).

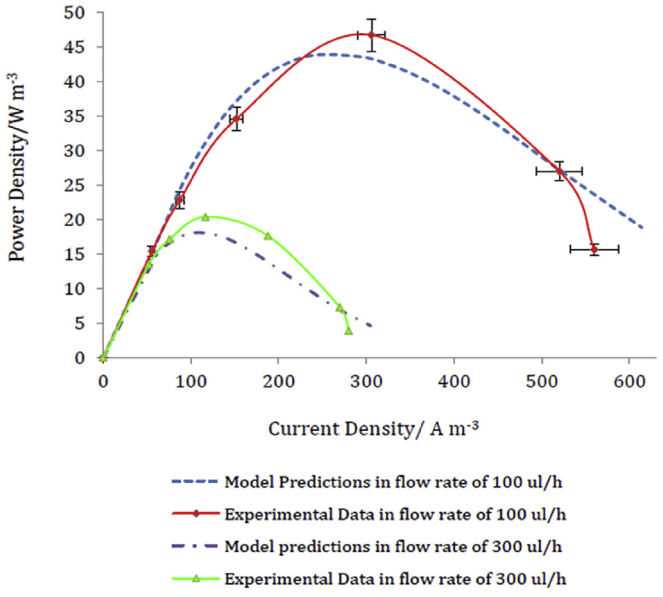

Fig. 2. Model verification with experimental data for glucose fed microfluidic MFC in different injection rates of substrate. External resistances of 100, 60, 30, 10, 2, 1 kΩ were used to obtain power density curves.

The distribution of suspended bacteria in the anolyte of microfluidic MFC is shown in Fig. 4. The trend of spatial distribution of suspended bacteria from the interior upper part (Z = 1000 μm) of microchannel to the interphase of anolyte/biofilm is descending indicating the adsorption of suspended bacteria to biofilm. This results from the response of quorum sensing to population density by secreting signaling molecules [45] and bacterial chemotaxis as experience of favorable chemical gradients of the substrate [46,47].

As shown in Fig. 4, the temporal variation of suspended bacteria indicates the consequence of two temporal characteristics of bacteria movement (including bacteria diffusion in the anolyte and the bacterial movement as a function of concentration gradient of the secreted sensing molecules) and the net growth rate of suspended bacteria is negligible as compared to the spatial variation of suspended bacteria. This means that the net growth rate of suspended bacteria compensates for their spatial variation.

4.3. Effect of external resistance on microfluidic MFC characteristics

It is also important to note that the effect of external resistance on the distribution of substrate concentration was inevitable. Fig. 5 shows the influence of this parameter on temporal distribution of dimensionless concentration of substrate in anolyte and biofilm.

It can be inferred from Fig. 5 that in lower external resistance, the reduction of substrate concentration in both anolyte and biofilm is more than that in higher external resistance. With respect to electron transfer mechanisms of *E. coli* and the point that more electron transfer proceeds substrate oxidation reaction and decreasing substrate concentration, so the reduction of substrate concentration with decreasing external resistance attributes to promoting more conductive path in biofilm matrix for cytochrome c to transfer electron or producing more electron shuttles in anolyte to achieve that. Moreover, the enhancement of bioelectrochemical activity of bacteria which led to more biodegradation of substrate by decreasing external resistance are shown in previous studies [48,49].

The effect of external resistance and other characteristics of the microfluidic MFC in dynamic condition were shown via radar diagram in Fig. 6.

As can be seen in Fig. 6, decreasing the external resistance not only significantly increases the produced current and dimensionless concentration of attached bacteria, the chemotactic velocity (as drift velocity toward an attractant or away from a repellent) is increased remarkably as well. By increasing the chemotactic velocity, the aggregation of bacterial cells to form biomass and/or to adhere electrode surface is implemented in shorter operating time of microfluidic MFC. These results and conclusions are in agreement with the experimental investigations of biofilm formation based on external resistances by Zhang et al. [49].

During continuous mode operation of MFC, the maximum value of potential in potential evolution curve is reported as sustained state of MFC. At higher external resistance more operating time is needed to reach sustained state compared to a lower external resistance [49,50]. The predicted value for biofilm thickness in Fig. 6 is associated with the sustained state of microfluidic MFC. So, the longer operating time is needed to approach sustained state in higher external resistance. As a consequence, at higher external resistance, more operating time led to predict the more value for

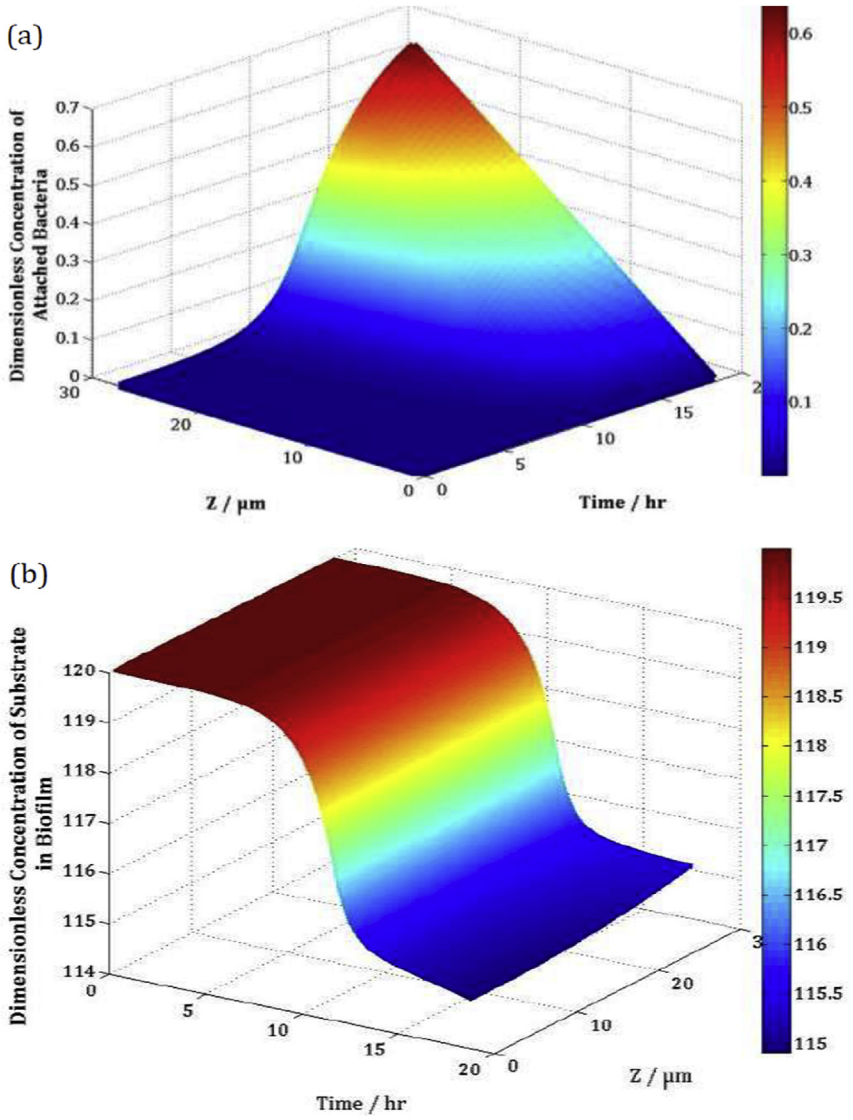

Fig. 3. The temporal and spatial distribution of biofilm and substrate concentrations in biofilm of microfluidic MFC. The microchannel diameter, the substrate flow rate and the external resistance were 1000 μm, 100 μl h^{-1} and 10 kΩ, respectively.

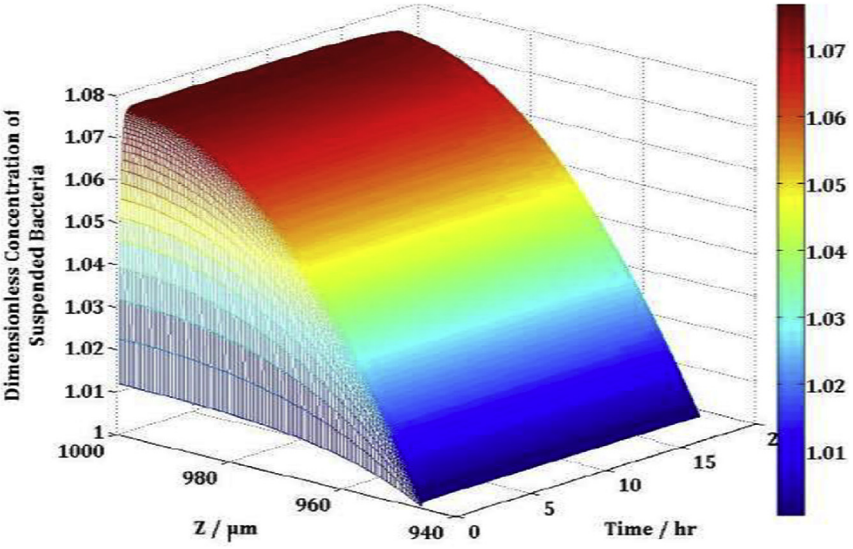

Fig. 4. The temporal and spatial distribution of dimensionless concentration of suspended bacteria in anolyte of microfluidic MFC. The microchannel diameter, the substrate flow rate and the external resistance were 1000 μm, 100 μl h^{-1} and 10 kΩ, respectively.

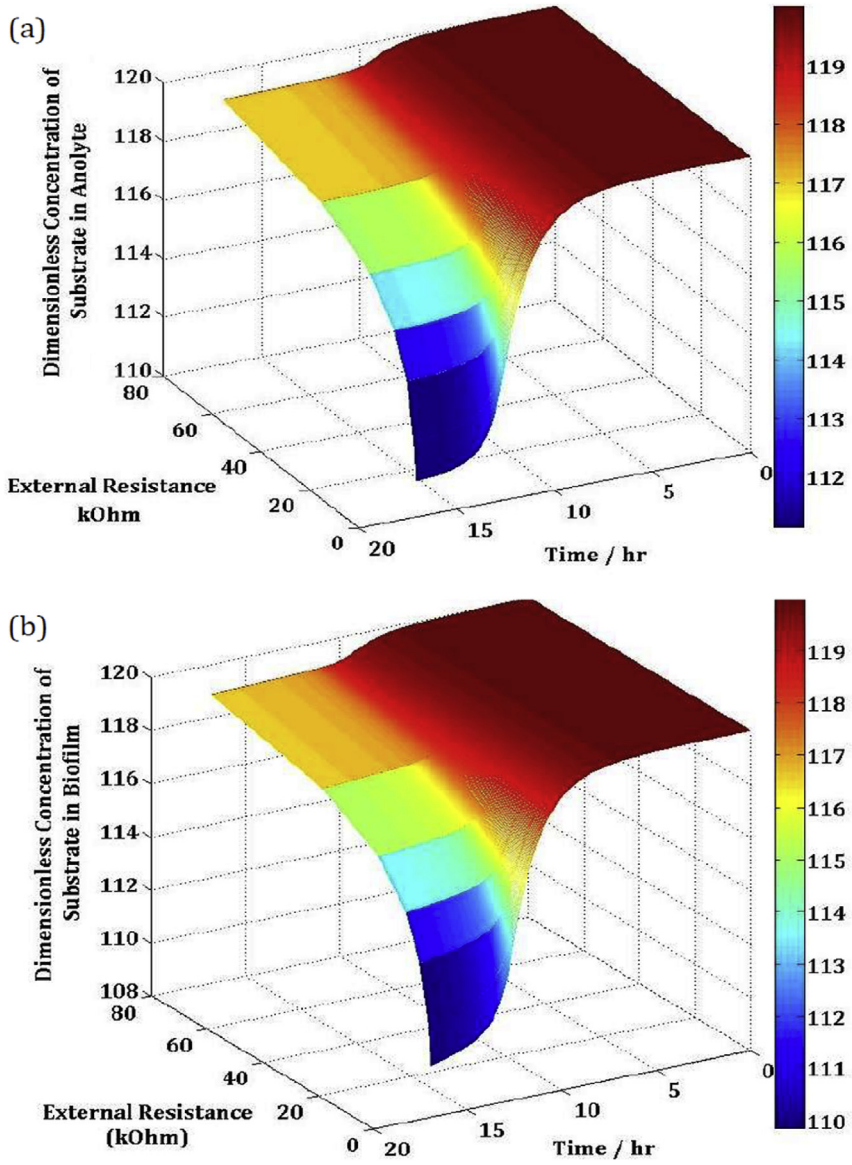

Fig. 5. Influence of external resistance on temporal distribution of dimensionless concentration of substrate in (a) anolyte and (b) biofilm. The microchannel diameter and the substrate flow rate were 1000 μm and 100 μl h^{-1}, respectively.

the microbial growth and biofilm thickness than that of the lower external resistance. Similar to chemotactic velocity, the concentration of secreted sensing molecules is a function of the operating time to approach sustained state and has a higher value at higher external resistances.

4.4. Effect of substrate flow rate on microfluidic MFC characteristics

In addition to external resistance, the influence of the substrate flow rate on microfluidic MFC characteristics is investigated. Fig. 7 shows that chemotactic velocity, produced current and concentration of attached bacteria have maximum values at a substrate flow rate of 100 μl h^{-1}.

The excess increase in flow rate had an adverse effect on bioelectricity production. This suggests that a disturbance in the bioelectrochemical activity of the bacteria could result from the increased substrate flow rate. A high flow rate at the microfluidic MFC anode when coupled with a high shear rate and other advective flow patterns that promote detachment from biofilm will decrease the number of biocatalysts on the electrode surface. This result and conclusion are consistent with the experimental results of the effect of flow rates on power generation of microfluidic MFC [20].

4.5. Effect of microchannel depth on microfluidic MFC performance

Fig. 8a shows the power density curves of glucose-fed microfluidic MFC in different hydraulic diameters of microchannel in an operating condition of 100 μl h^{-1} substrate flow rate and glucose concentration of 1200 mg l^{-1}.

The power density curve of microfluidic MFC with a microchannel depth of 1000 μm illustrates the experimental results, but other curves show the model predictions in different hydraulic diameters. As the hydraulic diameter of the microchannel is decreased, the power generation of microfluidic MFC increases significantly. In addition to the reduction of ohmic resistance by decreasing the microchannel depth, the significant enhancement in chemotactic velocity, as shown in Fig. 8b, is related to the increase

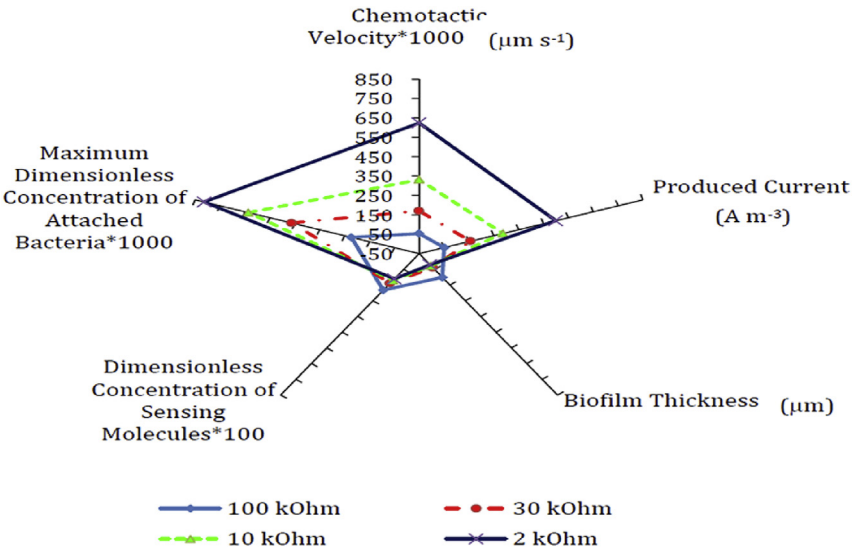

Fig. 6. Effect of external resistances on different characteristics of microfluidic MFC. The microchannel diameter and the substrate flow rate were 1000 μm and 100 μl h^{-1}, respectively.

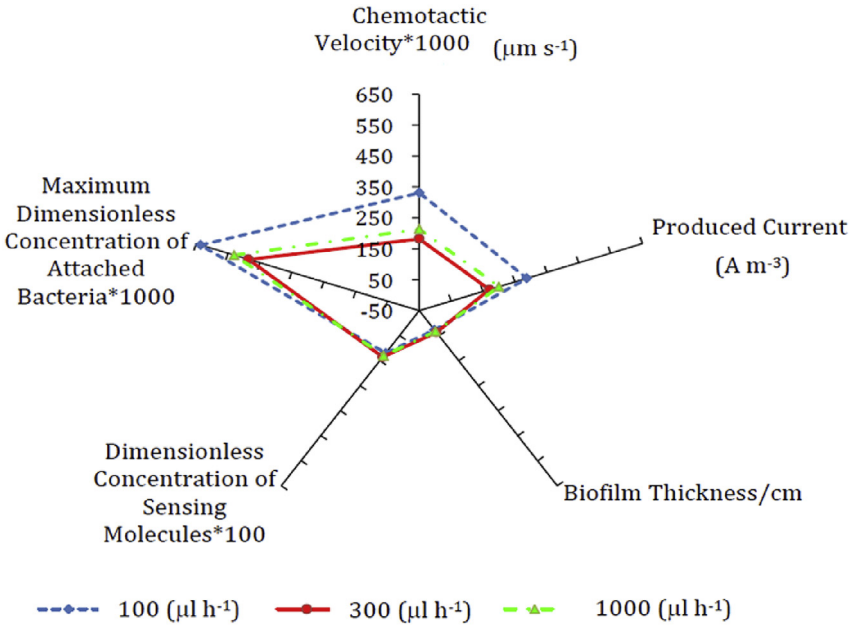

Fig. 7. Effect of substrate injection rate on different characteristics of microfluidic MFC. The microchannel diameter and the external resistance were 1000 μm and 10 kΩ, respectively.

in power generation of microfluidic MFC. The enhancement of chemotactic velocity leads to the shorter time span for aggregation of bacterial cells to form biomass that consequently facilitate electron transfer. Besides, as the hydraulic diameter decreases, then the linear velocity of the fluid in the anodic compartment increases. The increase in linear substrate velocity can induce enhancement of the mass transport of the substrate from decreased mass transport resistance between the bulk solution and the biofilm [51]. As a consequence, the reduction of ohmic resistance, the shorter time span for aggregation of bacterial cells and the increase in mass transfer of nutrients by decreasing the microchannel depth can be attributed to an increase in bioelectricity generation.

The evolution of chemotactic velocity shows that it increases abruptly after 10 h. This can be attributed to the occurrence of substantial variation in substrate concentration distribution, which was shown in Figs. 3 and 5. As chemotactic velocity is a strong function of substrate concentration gradient, any variation in this factor affects bacterial movement in anolyte.

5. Conclusion

The quantification of bacterial transport parameters to simulate biofilm formation and the suspended microorganisms' distribution in anolyte of microfluidic MFC was implemented numerically. The verification of the model prediction with the experimental data reveals the significant configurations of the present model with regard to electron transfer mechanisms as well as bacteria chemotaxis as foundation of biofilm formation are compatible with

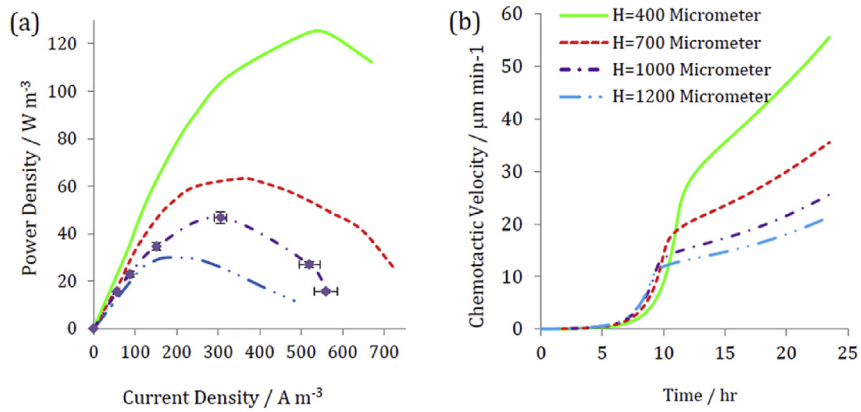

Fig. 8. (a) The power density curves of glucose-fed microfluidic MFC in different hydraulic diameters of microchannel and (b) the chemotactic velocity of bacteria versus operating time in different hydraulic diameters of microchannel. External resistances of 100, 60, 30, 10, 2, 1 kΩ were used to obtain power density curves. The substrate flow rate was 100 μl h^{-1}.

real conditions.

As the hydraulic diameter of microchannel is decreased, the power generation of microfluidic MFC increases significantly. The reduction of ohmic resistance, the shorter time span for aggregation of bacterial cells and the increase in mass transfer of nutrients by decreasing the microchannel depth can be attributed to an increase in bioelectricity generation.

The model showed that the concentration of attached bacteria is increased by increasing the distance from the anode that is attributed to the accessibility of nutrient on the biofilm surface in which the net growth rate of these bacteria would be higher.

Future research should focus on engaging multi-population as well as consider more biological and bioengineering interpretations of bacteria metabolic to improve the capability of microfluidic MFC model.

Acknowledgements

This research was supported by Sharif University of Technology, Vice President for Research Grant G930111.

Nomenclature

Symbols and description

A_{an}	Anode surface (m^2)
b_{ina}	Inactivation constant (day^{-1})
b_{res}	Respiration constant (day^1)
D	Dilution rate of microfluidic MFC
D_E	Diffusion coefficient of molecules (m^2 day^{-1})
$D_{s,f}$	Substrate diffusion coefficient in biofilm (m^2 day^{-1})
$D_{s,l}$	Substrate diffusion coefficient in the anolyte bulk (m^2 day^{-1})
E_{KA}	Half maximum rate potential (V)
F	Faraday's constant (96485 C mol−e $^{-1}$)
f_e^0	Fraction of energy-generating electrons (dimensionless)
H_{micro}	Height of microchannel (m)
I_{MFC}	Produced current in microfluidic MFC (A m^{-3})
i_0	Exchange current density in reference conditions (A m^{-2})
j	Current density (A m^{-2})
$J_{biofilm}$	Substrate flux from anolyte into biofilm (kg_{CODS} m^{-2} day^{-1})
k_{bio}	Biofilm conductivity (S m^{-1})
K_D	Receptor ligand dissociation constant (kg_{CODS} m^{-3})
K_M	Oxidized electron shuttles constant ($kg_{mediator}$ kg_{CODX}^{-1})
K_{Sd}	Monod half-saturation constants of substrate (kg_{CODS} m^{-3})
k_{sol}	Anolyte conductivity (S m^{-1})
l	The thickness of concentration boundary layer (m)
L_{f0}	Thickness of individual bacterium cell (m)
L_f	Biofilm thickness (m)
$M_{Mediator}$	Mediator molecular weight ($kg_{mediator}$ $kmole_{mediator}^{-1}$)
M_n	Mass of biomass particles (kg_{CODX})
M_{ox}	Oxidized mediators fraction per total mass of suspended bacteria ($kg_{mediator}$ kg_{CODX}^{-1})
M_{red}	Reduced mediators fraction per total mass of suspended bacteria ($kg_{mediator}$ kg_{CODX}^{-1})
M_{Total}	Total mediators fraction per total mass of suspended bacteria ($kg_{mediator}$ kg_{CODX}^{-1})
n	The number of electrons transferred per mole of mediator ($mole_{electrons}$ $mole_{mediators}^{-1}$)
p_0	Individual bacterial tumbling probability (day^{-1})
$q_{s,biofilm}$	Consumption rate of organic substrate in the biofilm (kg_{CODS} m^{-3} day^{-1})
$q_{s,bulk}$	Consumption rate of organic substrate in the anolyte (kg_{CODS} m^{-3} day^{-1})
$q_{s,max}$	Maximum consumption rate of organic substrate (kg_{CODS} kg_{CODX} $^{-1}$ day^{-1})
r_n	Biomass particles radius (m)
$r_{ina,bulk}$	Inactivation rate of suspended bacteria (kg_{CODX} m^{-3} day^{-1})
$r_{ina,biofilm}$	Inactivation rate of attached bacteria (kg_{CODX} m^{-3} day^{-1})
r_{res}	Endogenous respiration rate of bacteria in biofilm (kg_{CODX} m^{-3} day^{-1})
R	Universal gas constant (8.314 J mol^{-1} K^{-1})
R_{ext}	External resistance of microfluidic MFC (Ω)
R_{int}	Internal resistance of microfluidic MFC (Ω)
S_d	Substrate concentrations in porous biofilm (kg_{CODS} m^{-3})
$S_{d,bulk}$	Substrate concentrations in liquid bulk (kg_{CODS} m^{-3})
$S_{d,bulk}^0$	Substrate concentration at the inlet (kg_{CODS} m^{-2})
$S_{d,surf}$	Substrate concentration at the liquid bulk/biofilm interface (kg_{CODS} m^{-3})
S_E	Sensing molecules concentration (kg_{CODS} m^{-3})
S_{E_0}	Initial concentration of sensing molecules in anolyte (kg_{CODS} m^{-3})
$SR(t)$	Stickiness rate of suspended bacteria (kg_{CODX} m^{-3} day^{-1})
t	Time (day)
T	Anolyte temperature (K)
T_f	Rate of suspended bacteria sticking (m day^{-1})
V	Chemotactic velocity (m day^{-1})

V_{micro} Volume of microchannel (m^3)
X_a Density of biomass particles ($kg_{CODX}\ m^{-3}$)
z Spatial position (m)

Greek Symbol

α Sensing molecules production rate ($kg_{CODS}\ kg_{CODX}^{-1}\ day^{-1}$)
β Bacterial stickiness coefficient (m^{-1})
γ Microbial yields of bacteria ($kg_{CODX}\ kg_{CODS}^{-1}$)
γ_1 Electrons generated by substrate consumption ($mole_{electron}\ kg_{CODS}^{-1}$)
γ_2 Electrons generated by endogenous respiration ($mole_{electron}\ kg_{CODX}^{-1}$)
γ_M Oxidized mediator yield (kg-mediator $kgCOD_S^{-1}$)
δ Reduction or oxidation transfer coefficient (dimensionless)
η Local potential of anode surface (V)
η_{Act} Activation overpotential (V)
η_{Ohm} Ohmic overpotential (V)
η_{Con} concentration overpotential (V)
λ Sensing molecules degradation rate (day^{-1})
μ Random motility of bacteria ($m^2\ day^{-1}$)
μ_{s_0} Random motility coefficient of bacteria ($m^2\ day^{-1}$)
μ_{SE0} Random motility coefficients of sensing molecules ($m^2\ day^{-1}$)
ϑ Swimming speed of an individual bacterium ($m\ day^{-1}$)
τ Time conversion factor ($86400\ s\ day^{-1}$)
φ Direction persistence (dimensionless)
χ_0 Chemotactic sensitivity coefficient of substrate ($m^2\ day^{-1}$)
χ_{s_0} Chemotactic coefficients of sensing molecules ($m^5\ kg_{CODX}^{-1}\ day^{-1}$)
ψ_a Attached bacteria concentration ($kg_{CODX}\ m^{-3}$)
ψ_s Suspended bacteria concentration ($kg_{CODX}\ m^{-3}$)
ψ_{s_0} Initial concentration of suspended bacteria in the inlet of microchannel ($kg_{CODX}\ m^{-3}$)
R_{ohm} Ohmic resistance of microfluidic MFC (Ω)
ω Sensing molecules production rate in the boundaries ($m\ kg_{CODS}\ kg_{CODX}^{-1}\ day^{-1}$)

References

[1] R. He, R. Zhang, J. Yuan, Noise-induced increase of sensitivity in bacterial chemotaxis, Biophys. J. 111 (2016) 430–437.
[2] G. Micali, R.G. Endres, Bacterial chemotaxis: information processing, thermodynamics, and behavior, Curr. Opin. Microbiol. 30 (2016) 8–15.
[3] T. Ahmed, R. Stocker, Experimental verification of the behavioral foundation of bacterial transport parameters using microfluidics, Biophys. J. 95 (2008) 4481–4493.
[4] Nicholas A. Licata, B. Mohari, C. Fuqua, S. Setayeshgar, Diffusion of bacterial cells in porous media, Biophys. J. 110 (2016) 247–257.
[5] Y. Yang, D. Ye, J. Li, X. Zhu, Q. Liao, B. Zhang, Microfluidic microbial fuel cells: from membrane to membrane free, J. Power Sources 324 (2016) 113–125.
[6] Z. Chen, Y. Niu, S. Zhao, A. Khan, Z. Ling, Y. Chen, P. Liu, X. Li, A novel biosensor for p-nitrophenol based on an aerobic anode microbial fuel cell, Biosens. Bioelectron. 85 (2016) 860–868.
[7] C. Picioreanu, I.M. Head, K.P. Katuri, M.C. van Loosdrecht, K. Scott, A computational model for biofilm-based microbial fuel cells, Water Res. 41 (2007) 2921–2940.
[8] R. Sedaqatvand, M.N. Esfahany, T. Behzad, M. Mohseni, M.M. Mardanpour, Parameter estimation and characterization of a single-chamber microbial fuel cell for dairy wastewater treatment, Bioresour. Technol. 146 (2013) 247–253.
[9] A. Kato Marcus, C.I. Torres, B.E. Rittmann, Conduction-based modeling of the biofilm anode of a microbial fuel cell, Biotechnol. Bioeng. 98 (2007) 1171–1182.
[10] M.K. Alavijeh, M.M. Mardanpour, S. Yaghmaei, A generalized model for complex wastewater treatment with simultaneous bioenergy production using the microbial electrochemical cell, Electrochim. Acta 167 (2015) 84–96.
[11] M.K. Alavijeh, S. Yaghmaei, M.M. Mardanpour, A combined model for large scale batch culture MFC-digester with various wastewaters through different populations, Bioelectrochemistry 106 (2015) 298–307.
[12] M.K. Alavijeh, M.M. Mardanpour, S. Yaghmaei, One-dimensional conduction-based modeling of bioenergy production in a microbial fuel cell engaged with multi-population biocatalysts, Electrochim. Acta (2015) 151–163.
[13] R. Pinto, B. Srinivasan, A. Escapa, B. Tartakovsky, Multi-population model of a microbial electrolysis cell, Environ. Sci. Technol. 45 (2011) 5039–5046.
[14] R.P. Pinto, B. Srinivasan, M.F. Manuel, B. Tartakovsky, A two-population bio-electrochemical model of a microbial fuel cell, Bioresour. Technol. 101 (2010) 5256–5265.
[15] C. Picioreanu, M.C.M. van Loosdrecht, T.P. Curtis, K. Scott, Model based evaluation of the effect of pH and electrode geometry on microbial fuel cell performance, Bioelectrochemistry 78 (2010) 8–24.
[16] J. Li, G. Rosenberger, Z. He, Integrated experimental investigation and mathematical modeling of a membrane bioelectrochemical reactor with an external membrane module, Chem. Eng. J. 287 (2016) 321–328.
[17] Q. Ping, I.M. Abu-Reesh, Z. He, Mathematical modeling based evaluation and simulation of boron removal in bioelectrochemical systems, Sci. Total Environ. 569 (2016) 1380–1389.
[18] M. de los Ángeles Fernandez, M. de los Ángeles Sanromán, S. Marks, J. Makinia, A.G. del Campo, M. Rodrigo, F.J. Fernandez, A grey box model of glucose fermentation and syntrophic oxidation in microbial fuel cells, Bioresour. Technol. 200 (2016) 396–404.
[19] V.M. Ortiz-Martínez, M.J. Salar-García, A.P. de los Ríos, F.J. Hernández-Fernández, J.A. Egea, L.J. Lozano, Developments in microbial fuel cell modeling, Chem. Eng. J. 271 (2015) 50–60.
[20] M.M. Mardanpour, S. Yaghmaei, Characterization of a microfluidic microbial fuel cell as a power generator based on a nickel electrode, Biosens. Bioelectron. 79 (2016) 327–333.
[21] S. Cheng, H. Liu, B.E. Logan, Increased performance of single-chamber microbial fuel cells using an improved cathode structure, Electrochem. Commun. 8 (2006) 489–494.
[22] M. Peszynska, A. Trykozko, G. Iltis, S. Schlueter, D. Wildenschild, Biofilm growth in porous media: experiments, computational modeling at the pore-scale, and upscaling, Adv. Water Resour. 95 (2016) 288–301.
[23] G.E. Kapellos, T.S. Alexiou, S. Pavlou, Chapter 8-fluid-biofilm interactions in porous media A2-Kuznetsov, in: M. Sid, V. BeckerAndrey (Eds.), Heat Transfer and Fluid Flow in Biological Processes, Academic Press, Boston, 2015, pp. 207–238.
[24] J.-S. Guo, P. Zhang, Y.-P. Chen, Y. Shen, X. Hu, P. Yan, J.-X. Yang, F. Fang, C. Li, X. Gao, G.-X. Wang, Microbial attachment and adsorption–desorption kinetic of tightly bound extracellular polymeric substances on model organic surfaces, Chem. Eng. J. 279 (2015) 516–521.
[25] P. Zhang, J.-S. Guo, Y. Shen, P. Yan, Y.-P. Chen, H. Wang, J.-X. Yang, F. Fang, C. Li, Microbial communities, extracellular proteomics and polysaccharides: a comparative investigation on biofilm and suspended sludge, Bioresour. Technol. 190 (2015) 21–28.
[26] F. El Moustaid, A. Eladdadi, L. Uys, Modeling bacterial attachment to surfaces as an early stage of biofilm development, Math. Biosci. Eng. 10 (2013) 821–842.
[27] B.E. Rittmann, P.L. McCarty, Environmental biotechnology: principles and applications, Tata McGraw-Hill Educ., 2012.
[28] E.F. Keller, L.A. Segel, Traveling bands of chemotactic bacteria: a theoretical analysis, J. Theor. Biol. 30 (1971) 235–248.
[29] M.J. Tindall, P.K. Maini, S.L. Porter, J.P. Armitage, Overview of mathematical approaches used to model bacterial chemotaxis II: bacterial populations, Bull. Math. Biol. 70 (2008) 1570–1607.
[30] R.M. Ford, D.A. Lauffenburger, Analysis of chemotactic bacterial distributions in population migration assays using a mathematical model applicable to steep or shallow attractant gradients, Bull. Math. Biol. 53 (1991) 721–749.
[31] M.A. Rivero, R.T. Tranquillo, H.M. Buettner, D.A. Lauffenburger, Transport models for chemotactic cell populations based on individual cell behavior, Chem. Eng. Sci. 44 (1989) 2881–2897.
[32] F. El Moustaid, A. Eladdadi, L. Uys, Modeling bacterial attachment to surfaces as an early stage of biofilm development, Math. Biosci. Eng. 10 (2013) 821–842.
[33] E. Paul, J.C. Ochoa, Y. Pechaud, Y. Liu, A. Liné, Effect of shear stress and growth conditions on detachment and physical properties of biofilms, Water Res. 46 (2012) 5499–5508.
[34] J.B. Xavier, C. Picioreanu, M. Van Loosdrecht, A framework for multidimensional modelling of activity and structure of multispecies biofilms, Environ, Microbiol. 7 (2005) 1085–1103.
[35] A.R. Conn, N.I.M. Gould, P.L. Toint, Trust Region Methods, Society for Industrial and Applied Mathematics, 2000.
[36] W. Hundsdorfer, J.G. Verwer, Numerical Solution of Time-dependent Advection-diffusion-reaction Equations, Springer Science & Business Media, 2003.
[37] M. Poccia, A. Beccaria, R. Dondo, Modeling the microbial growth of two Escherichia coli strains in a multi-substrate environment, Braz. J. Chem. Eng. 31 (2014) 347–354.
[38] D. Green, R. Perry, Perry's Chemical Engineers' Handbook, 18 ed., McGraw-Hill Education, New York, USA, 2007.
[39] T. Zhang, H. Fang, Effective diffusion coefficients of glucose in artificial biofilms, Environ. Technol. 26 (2005) 155–160.
[40] H. Beyenal, J.T. Babauta, Biofilms in Bioelectrochemical Systems: from Laboratory Practice to Data Interpretation, John Wiley & Sons, 2015.
[41] P. Cluzel, M. Surette, S. Leibler, An ultrasensitive bacterial motor revealed by monitoring signaling proteins in single cells, Science 287 (2000) 1652–1655.
[42] B.E. Logan, Microbial Fuel Cells, John Wiley & Sons, 2008.
[43] R. Sedaqatvand, M.N. Esfahany, T. Behzad, M. Mohseni, M.M. Mardanpour,

Parameter estimation and characterization of a single-chamber microbial fuel cell for dairy wastewater treatment, Bioresour. Technol. 146 (2013) 247–253.
[44] M. Karimi Alavijeh, M.M. Mardanpour, S. Yaghmaei, Modeling of multi-population microbial fuel and electrolysis cells based on the bioanode potential conditions, Iran. J. Hydrogen & Fuel Cell 1 (2015) 247–260.
[45] A. Yajima, Chapter 10-recent advances in the chemistry and chemical biology of quorum-sensing pheromones and microbial hormones, in: R. Atta ur (Ed.), Studies in Natural Products Chemistry, Elsevier, 2016, pp. 331–355.
[46] R. He, R. Zhang, J. Yuan, Noise-induced increase of sensitivity in bacterial chemotaxis, Biophys. J. 111 (2016) 430–437.
[47] G. Micali, R.G. Endres, Bacterial chemotaxis: information processing, thermodynamics, and behavior, Curr. Opin. Microbiol. 30 (2016) 8–15.
[48] M.M. Mardanpour, M.N. Esfahany, T. Behzad, R. Sedaqatvand, F. Sharifi, F. Naderi, Factors affecting the performance of single chamber microbial fuel cell using a novel configuration, Iran. J. Energy Environ. 4 (2013) 343–347.
[49] L. Zhang, X. Zhu, J. Li, Q. Liao, D. Ye, Biofilm formation and electricity generation of a microbial fuel cell started up under different external resistances, J. Power Sources 196 (2011) 6029–6035.
[50] M.M. Mardanpour, M.N. Esfahany, T. Behzad, R. Sedaqatvand, Single chamber microbial fuel cell with spiral anode for dairy wastewater treatment, Biosens. Bioelectron. 38 (2012) 264–269.
[51] D. Ye, Y. Yang, J. Li, X. Zhu, Q. Liao, B. Deng, R. Chen, Performance of a microfluidic microbial fuel cell based on graphite electrodes, Int. J. Hydrogen Energ 38 (2013) 15710–15715.